Mechanisms of basal ice formation in polar glaciers: An evaluation of the apron entrainment model

Sean Fitzsimons,[1] Nicola Webb,[1] Sarah Mager,[1] Shelley MacDonell,[1] Regi Lorrain,[2] and Denis Samyn[2]

[1]   Previous studies of polar glaciers have argued that basal ice can form when these glaciers override and entrain ice marginal aprons that accumulate adjacent to steep ice cliffs. To test this idea, we have studied the morphology, structure, composition, and deformation of the apron and basal ice at the terminus of Victoria Upper Glacier in the McMurdo dry valleys, which are located on the western coast of the Ross Sea at 77°S in southern Victoria Land, Antarctica. Our results show that the apron has two structural elements: an inner element that consists of strongly foliated ice that has a steep up-glacier dip, and an outer element that lacks a consistent foliation and has a down-glacier, slope-parallel dip. Although strain measurements show that the entire apron is deforming, the inner element is characterized by high strain rates, whereas relatively low rates of strain characterize the outer part of the apron. Co-isotopic analyses of the ice, together with analysis of solute chemistry and sedimentary characteristics, show that the apron is compositionally different from the basal ice. Our observations show that aprons may become deformed and partially entrained by advancing glaciers. However, such an ice marginal process does not provide a satisfactory explanation for the origin of basal ice observed at the ice margin. Our interpretation of the origin of basal ice is that it is formed by subglacial processes, which are likely to include deformation and entrainment of subglacial permafrost.

1.   Introduction

[2]   Basal ice can be defined as a relatively thin layer of ice that forms at the bed of glaciers. It is physically and compositionally distinctive from ice that is formed from the compaction of snow because it is modified by thermal, deformation and hydraulic processes that operate at the beds of glaciers. Typically basal ice contains debris eroded from the glacier bed, relatively high solute concentrations and gas concentrations that are different from atmospheric values. Understanding basal ice is a significant issue in glaciology and geomorphology because it acts as a rheological control on glacier behavior and it has the potential to provide insights into subglacial geologic processes. Consequently, knowledge and understanding of the characteristics of basal ice has the potential to bridge studies of modern glaciological processes and formerly glaciated landscapes.

[3]   Debris-bearing ice has been observed at the base of many polar glaciers that have basal temperatures lower than

the pressure-melting point (i.e., glaciers that are cold-based) [*Holdsworth*, 1969, 1974; *Koerner*, 1989; *Fitzsimons*, 1996, 2006; *Cuffey et al.*, 2000a]. These observations provide evidence of subglacial erosion processes which challenge the prevalent assumption in the geomorphological literature that cold-based glaciers are not significant agents of landscape change [e.g., *Sugden*, 2006; *Kleman et al.*, 2006]. The apparent tension between observations of basal ice in cold-based glaciers and the geomorphological literature may be resolved by the apron entrainment model of basal ice formation [*Shaw*, 1977] which suggests that debris is entrained at ice margins rather than by subglacial erosion. This model, which is derived from observations of the morphology and structure of the margins of polar glaciers, argues that the basal ice zone in polar glaciers is formed as accumulations of ice and debris (aprons) are overridden by advancing glaciers.

[4]   The margins of polar glaciers that terminate on land are often characterized by dramatic cliffs below which frontal aprons of snow, ice blocks, refrozen melt water and debris accumulate [*Goldthwait*, 1971; *Hooke*, 1973; *Sharp*, 1984]. The location of the apron, adjacent to the ice cliff (Figure 1), means that the apron may form an obstruction to glacier flow and may be overridden during ice advances. On the basis of observations of ice margins in the McMurdo dry valleys, *Shaw* [1977] suggested that this

---

[1]Department of Geography, University of Otago, Dunedin, New Zealand.
[2]Laboratoire de Glaciologie, Département des Sciences de la Terre et de l'Environnement, Université Libre de Bruxelles, Bruxelles, Belgium.
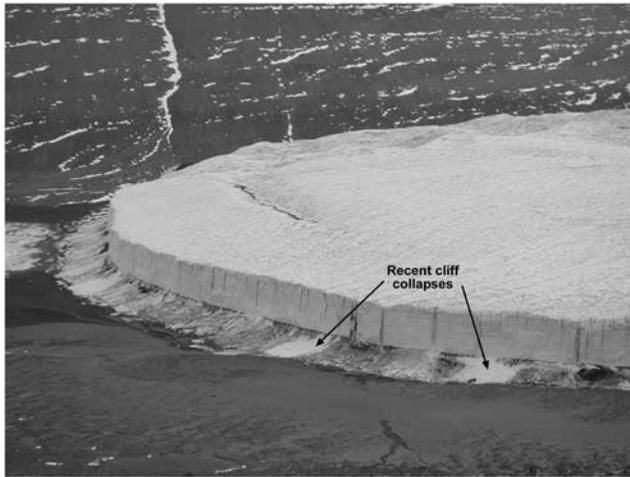
Figure 1. Left margin of Victoria Upper Glacier showing the apron that has formed at the foot of the terminal cliff. Ice from recent cliff collapses can be seen on the left of the photograph. The cliff is approximately 40 m high.

process plays a significant role in the formation of basal ice and cited the following features as evidence of the process: the bubbly appearance and foliation of basal ice; sorting of the debris inherited from the apron; the approximate conformity of the top of the basal debris and the height of the frontal apron; and tilting of terraces formed at the glacier margin [*Shaw*, 1977, Figure 5]. Subsequent investigation of the distribution and characteristics of some debris entrained by glaciers in the Canadian high Arctic and Alaska concluded that the structure and arrangement of the debris was consistent with Shaw's apron entrainment model [*Evans*, 1989; *Sharp et al.*, 1994]. However, Evans concluded that the process of apron overriding remains imperfectly understood. Almost 30 yr after Shaw's initial descriptions the apron entrainment mechanism for basal ice formation has yet to be thoroughly evaluated. Understanding the process is important because if basal ice in cold-based glaciers is derived from apron entrainment it cannot be regarded as evidence of subglacial erosion. If this proves to be the case the divergent views of the role of cold-based glaciers as geomorphological agents outlined above may be reconciled. Alternatively, if apron entrainment does not provide a satisfactory explanation of the origin of the basal ice, we may be able to clarify the source of basal ice and address the question of whether cold-based glaciers can be significant agents of erosion.

[5] The purpose of this paper is to test Shaw's apron entrainment hypothesis through an investigation of the structure, composition and deformation of an apron at the margin of Victoria Upper Glacier, McMurdo dry valleys. The specific question we ask is whether the distinctive debris-bearing ice that crops out at the foot of the terminal cliffs of cold-based glaciers is derived from entrainment and attenuation of the apron. In this paper we use the term basal ice for the debris-bearing ice that crops out at the foot of ice marginal cliffs and apron ice for material that has accumulated at the ice margin. We maintain this distinction for the convenience of testing the hypothesis that basal ice is derived from the apron, recognizing that if the apron is completely overridden it would become a form of basal ice.

2. Methods

[6] To test the validity of the apron entrainment model we have studied the morphology, structure, composition and deformation of the apron at the margin of Victoria Upper Glacier (Figure 1). The topography of the apron was surveyed using a compass, clinometer and tape measure, and subsurface structures were mapped using a PulseEkko ground-penetrating radar (GPR). The radar was used in a broadside configuration (antennae perpendicular to the survey line) with 100 and 50 MHz antennae. The radar wave propagation velocity of the ice and debris was determined by undertaking common midpoint (CMP) surveys and these were used to calculate depth from the two-way travel time. Eight radar lines were surveyed perpendicular to the ice margin, crossing the frozen lake, delta, and apron slope up to the foot of the ice cliff. The GPR data were filtered to remove the transient signal associated with the diffusion of the low-frequency component of the radar pulse (dewowed), migrated using a scale factor of 0.2 and propagation velocities from the CMP surveys, and topographically corrected to produce the profiles.

[7] Subsurface structures were also examined in a tunnel excavated through the apron using electric chainsaws and demolition hammers. The tunnel was oriented parallel to ice flow and extended 40 m from the toe of the apron to a point beneath the ice cliff. Within the tunnel continuous records of ice deformation were obtained using linear variable displacement transducers (LVDTs) and potentiometers logged every 60 min using Campbell Scientific data loggers powered by deep cycle batteries that were charged with a wind generator. In addition, strain and displacement measurements were made using plumb lines and strain arrays. Each strain array consisted of a rectangle of stainless steel bolts with cones milled into their heads. Measurements of the distances between the bolts were obtained using a digital caliper with a precision of 0.01 mm. The caliper was accurately positioned on the bolts by attaching conical pins to the caliper jaws, which fitted tightly into the cones milled into the bolts. The arrays were resurveyed episodically for up to 3 yr. During this time there was some bulging of the tunnel walls, which could introduce errors related to differences in closure rates with increasing overburden through the length of the tunnel. To minimize these errors, the strain arrays were mounted on the tunnel walls 50 mm above the floor of the tunnel where wall bulging was minimal. The effect of wall bulging was measured by mounting LVDTs parallel and perpendicular to the walls over a period of 1 yr. The flow-perpendicular LVDTs recorded no detectable displacement whereas the LVDTs mounted parallel to flow recorded displacements that increased with increasing distance into the tunnel. Strain rates were calculated from the corners of triangles defined from the strain arrays using a numerical calculation of a Mohr circle on the basis of the method outlined by *Ramsay* [1967] and used in glaciology by *Hambrey and Muller* [1978] and *Hambrey et al.* [1980]. We have followed the convention for principal strain rates that $\dot{\varepsilon}_1 \geq \dot{\varepsilon}_3$, that extension is positive and $\dot{\varepsilon}_3$ is always

Table 1. Principal Strain Rates in the Tunnel

Distance Into Tunnel, m	$\dot{\varepsilon}_1$	$\dot{\varepsilon}_2$	$\dot{\varepsilon}_3$[a]	$\dot{\gamma}$[b]	Ice Thickness, m
8	0.0122	−0.0143	0.0021	−0.0143	1.5
13.6	0.0388	−0.0096	−0.0292	−0.0150	3
19.2	0.0127	−0.0128	0.0001	−0.0128	5
25.8	0.0228	−0.0257	0.0029	−0.0257	6.5
37	0.0409	−0.0459	0.0050	−0.07428	8

[a]Where $\dot{\varepsilon}_1 + \dot{\varepsilon}_2 + \dot{\varepsilon}_3 = 0$.

[b]Where $\dot{\gamma} = \frac{\dot{\varepsilon}_1 - \dot{\varepsilon}_2}{2}$.

horizontal [*Sharp et al.*, 1988]. Shear strain rate has been calculated as $\dot{\gamma} = \frac{\dot{\varepsilon}_1 - \dot{\varepsilon}_2}{2}$ [*Sharp et al.*, 1988]. If no wall bulging occurred $\dot{\varepsilon}_3$ would be zero, which is not the case (Table 1). However, $\dot{\varepsilon}_3$ is about an order of magnitude less than $\dot{\varepsilon}_1$, and both $\dot{\varepsilon}_1$ and $\dot{\gamma}$ increase into the tunnel (Table 1). Consequently we conclude that tunnel closure has not introduced major errors to the calculation of strain rates.

[8] Samples of basal ice were collected using a chainsaw, with basal ice cut from the foot of the ice cliff, and apron ice samples from locations in the tunnel. The relatively low numbers of samples (20) mean that it is possible that there is a systematic bias between what was sampled and the relative abundance of the different types of ice. However, visual inspection of the samples suggested that a representative sample of debris-bearing and clean ice samples was captured by the random sampling scheme. Although the apron ice is likely to be a mélange of material, a conglomerate structure was visible only in the first 4 m of the tunnel, beyond which the ice structure in the tunnel was homogenized. A sampling scheme using random numbers to locate ice samples in the tunnel was chosen in order to test the hypothesis that the basal ice is derived from homogenized apron ice. Following collection, the frozen samples were returned to the laboratory where they were subsampled in a freezer using a band saw to produce samples of about 50 ml. Although there was some variability in sediment concentration in the basal ice and apron samples, all subsamples contained some dispersed debris.

[9] After subsampling, the ice was melted at room temperature within 10 min of being cut and immediately filtered with 0.45 μm cellulose nitrate filter paper. Several melted samples were left in contact with sediment for up to 2 hours to examine whether the solute load of the water

Table 2. Precision, Detection Limits, and Accuracy of Solute Measurements

	NO$_3^-$	K$^+$	Na$^+$	Ca^{2+}	Mg^{2+}	Cl$^-$
Precision[a]	0.52	0.06	0.27	0.26	0.04	0.13
Detection limit[b]	0.45	0.18	0.82	0.78	0.12	0.38
Accuracy[c]	0.26	0.01	−0.01	−0.01	−0.01	−0.09
Coefficient of variation[d]	0.03	0.01	0.05	0.05	0.02	0.01

[a]Standard deviation of repeated assays laboratory of standards.

[b]Instrument detection limit: standard deviation of 7 assays of a laboratory close to the detection limit multiplied by 3.

[c]Concentration of laboratory standard minus the mean of laboratory assays of the standard.

[d]Standard deviation of assays of laboratory standards divided by the mean.

increased with longer exposure times. These experiments demonstrated that after the extended exposure time there was no detectable increase in solute concentrations. The data from this study show that ice samples with greater volumes of debris have lower solute concentrations, which suggests that the solutes were held in the ice rather than on particles. A Foss FIAStar 500 Flow Injection Analyser (FIA) was used to measure the concentrations of chloride and nitrate, and a Varian Spectra 220FS Atomic Absorption Spectrophotometer (AAS) was used to measure the concentrations of sodium, magnesium, potassium and calcium. We have not reported sulphate concentrations because of difficulties experienced with an ion chromatograph. The detection limits of the FIA and AAS vary between 0.12 for Mg^{2+} to 0.78 for Ca^{2+} and precision ranges from 0.04 to 0.5 (Table 2). Hydrogen isotope ratios (δD) were measured using a VG Sira Isotope Ratio Mass Spectrometer using the chromium reduction technique described by *Donnelly et al.* [2001]. The samples were assayed six times per injection to achieve a precision of 0.5‰. The oxygen isotopes were analyzed using the online reduction of liquid water to carbon dioxide by nickelized carbon with a Eurovector EA mass spectrometer according to the method described by *Farquhar et al.* [1997]. Each sample was measured four times, and the first injection was ignored to reduce any memory effects from previously injected samples. Samples were measured against a standard laboratory reference gas and calibrated using SLAP and SMOW international standards. The precision for this method is 0.1‰. The reported ratios are relative to VSMOW.

3. Results

[10] The margin of Victoria Upper Glacier is characterized by a 40 m cliff, below which a continuous ice apron has formed (Figure 1). The apron has an average slope length of

Figure 2. Profile of the apron and cliff at the left margin of Victoria Upper Glacier showing the slightly concave slope and the abrupt change in slope at the foot of the ice cliff. Patches of gravel on the upper part of the apron have formed from melting of debris from the adjacent basal ice. The dirty vertical line on the ice cliff marks the position of a stream of fine debris from the glacier. The apron slope is about 50 m long.
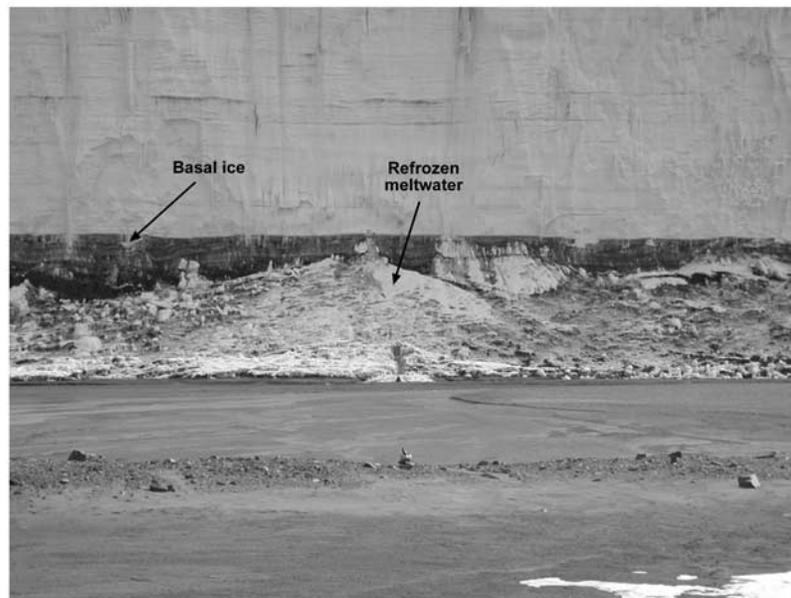
Figure 3. Photograph of the apron surface showing uneven slopes produced by summer ablation and eolian sand blown onto the apron surface, and accumulation of debris from basal ice melt.

50 m and is slightly concave upward, with slopes ranging from 10° at the apron foot to 40° adjacent to the cliff (Figure 2). The morphology of the slope ranges between a smooth surface formed by refreezing of melt water, to rough accumulations of large ice blocks from recent cliff collapses (Figure 3). Patches of coarse angular gravel at the top of the apron were deposited by melt of basal ice and thin accumulations of eolian sand have been deposited on the lower slopes (Figures 2 and 3).

[11] The first 4 m of the tunnel is dominated by a conglomerate ice texture (Figure 4), which consists of erratically oriented blocks of bubbly, foliated ice in a matrix of dense, bubble-free ice with occasional sediment particles. A similar texture has been observed in basal ice formed by apron overriding during a surge-induced ice advance at Variegated Glacier [*Sharp et al.*, 1994]. We interpret this assemblage as the product of cliff calving followed by partial melting and refreezing. Between 4 and 20 m the ice has a homogeneous appearance, i.e., it was massive, white ice with very low volumes of dispersed debris. Beyond 20 m in the tunnel and on the upper part of the apron the homogeneous appearance gives way to a layered structure that dips in an up-glacier direction between 35° and 65° (Figure 5). This ice and the ice exposed at the foot of the cliff are finely laminated, strongly bubble foliated and contain predominantly sand-sized debris arranged in grain-thick laminae. Occasional angular pebble to cobble-sized particles and blocks of frozen sand are strongly imbricated parallel to glacier flow (Figure 5).

[12] GPR profiles surveyed across the proglacial area reveal numerous hyperbolae that are probably subsurface boulders (e.g., Figures 6a and 6b). All of the radar profiles show that topset beds of the ice-marginal delta extend beneath the glacier apron (Figure 6). Some of the topset beds (e.g., Figure 6c) appear to have experienced shortening, which is consistent with compressive deformation at the glacier terminus. The internal structure of the apron is dominated by slope-parallel, layers that dip in a down-glacier direction, which is consistent with observations of surface layering. In contrast, further up the apron the internal structure is dominated by layering that has an up-glacier dip (Figure 7). Shear strain rates increase into the tunnel except at 20 m where there is a slight decease (Figure 8). The increase in shear strain rates is coincident with increasing ice thickness (Table 1). Ice velocities, measured 2 m above the floor of the tunnel were 0.9 m/a at 20 m, 1.6 m/a at 30 m and 2.2 m/a at the end of the tunnel (40 m).

[13] The solute concentrations of ice samples from the apron are lower than those from basal ice (Table 3) and there are statistically significant differences between values

Figure 4. Backlit thick section (10 mm thick) of apron ice showing the conglomerate texture of blocks of meteoric-origin ice that are cemented by refrozen melt water. The gloved fingers are 20 mm wide.

Figure 5. Steeply dipping (65°) basal ice exposed on the upper part of the apron and the lower part of the terminal cliff. The angular particles up to 150 mm in diameter are oriented parallel to ice flow. The left side of the photograph shows a thin refrozen ice layer concealing the basal ice.

for potassium, sodium, calcium and magnesium (Mann-Whitney U test with 95% confidence limits). In contrast, the sediment concentrations of the apron ice are greater than values from the basal ice (Table 3). The high standard deviation associated with the sediment concentration of the apron ice reflects a bimodal distribution with some samples containing very little debris and a few samples containing up to 20% by volume.

[14] Sixteen samples of ice from the glacier surface were collected to calculate the local meteoric water line (LMWL) which is $\delta D = 8.45\ \delta^{18}O + 12.18$ ($r^2 = 0.98$, slope standard error ± 0.1, Figure 9). This line is statistically indistinguishable from other meteoric water lines in the McMurdo dry valleys [e.g., Suess Glacier; *Lorrain et al.* [1999]] and the world meteoric water line [*Rozanski et al.*, 1993]. Regression of the co-isotopic data from basal ice samples yielded the equation: $\delta D = 8.56\ \delta^{18}O + 15.71$ ($r^2 = 0.88$, slope standard error ± 0.1, Figure 10). This line is statistically indistinguishable from the LMWL. By contrast samples from the apron plot on the line $\delta D = 6.6\ \delta^{18}O - 50.71$ ($r^2 = 0.80$, slope standard error ± 0.16) which has a significantly lower gradient than the LMWL and samples from basal ice (Figure 10). The isotope data are summarized in Table 4. Although the deuterium excess of the samples is highly variable the environmental significance of such variability in basal ice remains unknown [*Souchez and Lorrain*, 2006].

4. Discussion

4.1. Interpretation

[15] Surface and subsurface mapping show there is a structural discontinuity between the inner and outer parts of the apron. The outer part is characterized by a "conglomerate" ice texture, slope-parallel layering and relatively low strain rates, whereas the inner part of the apron is characterized by strongly foliated ice, steep up-glacier layering and relatively high shear strain rates. This discontinuity is also reflected in isotopic data.

[16] Plotting the isotopic data on δD-$\delta^{18}O$ diagrams shows that englacial ice plots on a meteoric water line (Figure 9) and that the isotopic ratios from the apron and
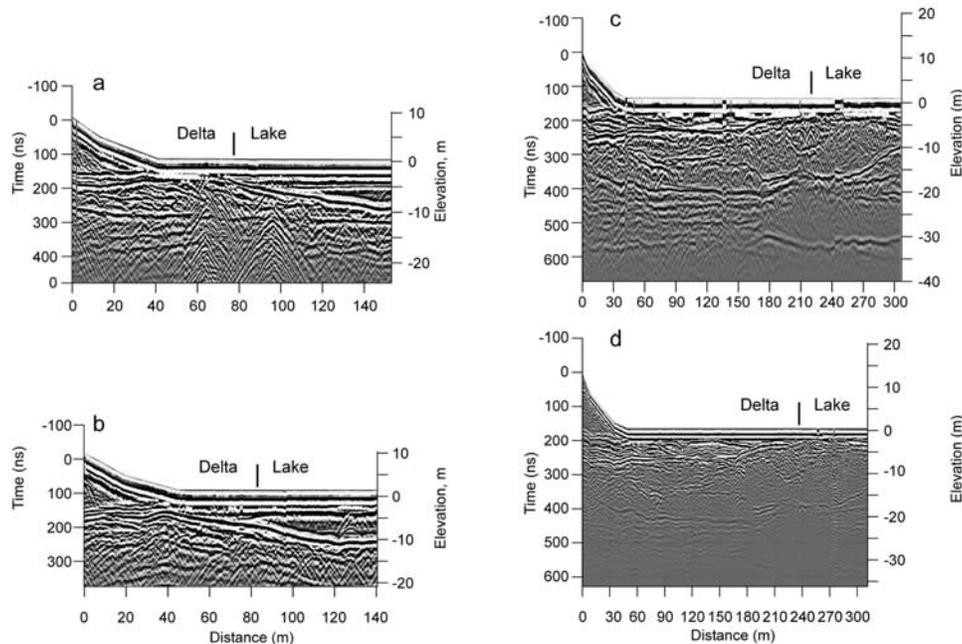

Figure 6. (a–d) Ground-penetrating radar profiles of the glacier terminus showing planar-bedded sediments underlying the apron. The dominant structure in the apron dips in the same direction of the surface slope. Shortening of the sediments beneath the apron at around 30 m in Figures 6c and 6d suggests compressional deformation close to the ice margin. Numerous hyperbolae beneath the delta and lake in Figures 6a and 6b have probably been produced by buried boulders.
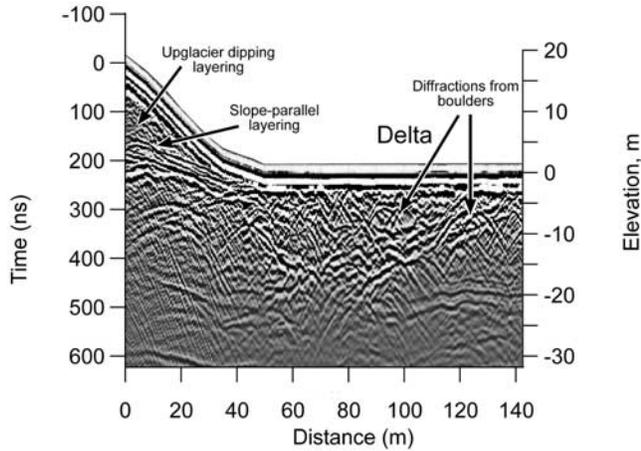
Figure 7. Detail of a GPR profile showing up-glacier dipping layering in the upper part of the apron and slope-parallel layering in the outer part of the apron. Numerous hyperbolae beneath the delta (60 to 140 m) record the presence of boulders.

basal ice overlap with each other (Figure 10). Regression lines show that the basal ice plots parallel to the meteoric water line (Figures 9 and 10) and ice from the apron has a slope of 6.6. Following the work of *Jouzel and Souchez* [1982] and *Souchez and Jouzel* [1984] we calculate a "freezing slope" for an open system to derive the isotopic signature produced by freezing water with a given isotopic composition:

$$S = \frac{\alpha[(\alpha - 1)(1000 + \delta_i D)]}{\beta[(\beta - 1)(1000 + \delta_i^{18}O)]} \qquad (1)$$

Where $\delta_i D$ and $\delta_i^{18}O$ is the isotopic composition of the parent water and α and β, the values of the ice-water equilibrium fractionation coefficients taken as 1.0212 and 1.00291 for δD and $\delta^{18}O$ respectively [*Lehmann and Siegenthaler*, 1991].

[17] To calculate a freezing slope we take the intersection to the LMWL and the apron ice slope as the isotopic composition of the parent water as suggested by *Souchez and Jouzel* [1984]. This value (−269.1‰ and −33.0‰ for δD and $\delta^{18}O$ respectively) yields a slope of 5.60, which lies outside the 95% confidence interval for the empirically determined slope for the apron ice (6.6 ± 0.36). Thus apron ice has not formed by simple freezing of water derived from this meteoric source. However, this approach assumes that all samples are from water of an identical isotopic composition [*Sharp et al.*, 1994]. An alternative, and perhaps more realistic, approach is to calculate a "freezing envelope" that can be modeled supposing that apron ice could be derived from melting and refreezing of any initial ice encountered at the glacier margin. Such a model can be calculated from the complete isotopic range encountered at the glacier terminus (δD −261.7 and $\delta^{18}O$ −33.5 to δD −226.7‰ and $\delta^{18}O$ −31.2‰). This produces a "freezing envelope" with slopes between 5.66 and 5.47. Clearly the ice from the apron, which plots on a slope of 6.6, lies outside this envelope. The simplest interpretation of a co-isotopic slope that lies between the LMWL and a freezing slope is that the apron consists of a mixed population of meteoric ice and melted and refrozen ice. This interpretation is consistent with the "conglomerate" texture observed from thick sections of the apron (Figure 4), which shows unaltered meteoric ice blocks together with ice formed by refreezing of melt water. Once such a mixed origin ice forms there is no known mechanism for it to evolve isotopically back toward the meteoric slope that characterizes the basal ice. Consequently, the isotopic data suggest the basal ice is not derived from the apron ice.

[18] Taken together the co-isotopic and solute data demonstrate that the apron ice is compositionally distinct from the basal ice. These differences suggest that it is unlikely that the basal ice is derived from entrainment of the glacier apron. Furthermore, the steep dip of the basal ice (Figure 5) suggests that it is being forced to flow over the apron. The contrasting compositional data together with structural data have shaped our interpretative model, which shows the apron as a proglacial feature (Figure 11). By contrast, the basal ice has a distinctive composition, debris
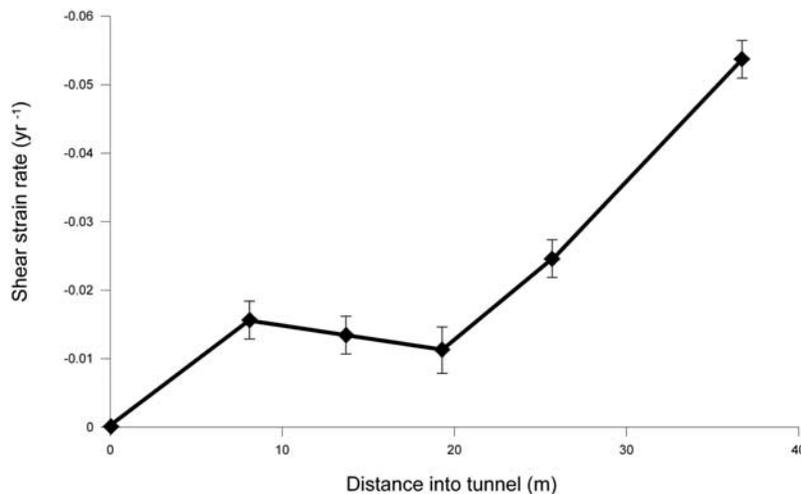

Figure 8. Shear strain rates ($\dot{\gamma} = \frac{\dot{\varepsilon}_1 - \dot{\varepsilon}_2}{2}$) calculated from strain arrays in the tunnel. The error bars represent uncertainty related to the precision of the digital caliper (±0.01 mm).

Table 3. Solute Data From the Apron and Basal Ice[a]

	NO_3^-	K^+	Na^+	Ca^{2+}	Mg^{2+}	Cl^-	Total Dissolved Solids	Sediment Concentration, $g\ L^{-1}$	n
Apron, mg/L	0.28 (0.06)	0.72 (0.12)	0.70 (0.05)	0.35 (0.07)	0.04 (0.01)	1.39 (0.75)	3.76 (0.36)	9.36 (2.96)	24
Basal ice, mg/L	0.28 (0.07)	1.03 (0.21)	0.87 (0.09)	0.74 (0.17)	0.07 (0.01)	1.81 (0.28)	5.08 (0.62)	1.78 (2.14)	20

[a]The data are averages and standard deviations in parentheses. Units are mg/L.

content and structure, which suggests that it is derived from subglacial processes. Compression at the ice margin at least partly driven by the glacier flowing into the apron has resulted in uplift of the basal ice, which crops out at the foot of the terminal cliff and on the upper slope of the apron. The basal ice is underlain by a wedge-shaped mass of ice and debris that has accumulated at the glacier margin. Although this wedge undergoes deformation it remains structurally and compositionally distinct from the overlying basal ice. Consequently, we conclude that there are two distinct ice types: one derived from a subglacial position and stratigraphically above the glacier apron and the other derived from ice marginal processes in which the proglacial apron has been overridden and partially entrained by the glacier (Figure 11).

4.2. Comparison with Previous Descriptions of Aprons

[19] In a study of the structure and behavior of the margin of the Barnes Ice Cap *Hooke* [1973] used ice crystal fabric data to identify an up-glacier thinning wedge of deformed superimposed ice beneath the ice margin. This author argued that an ice-cored "inner" moraine forms at the contact between the superimposed ice and the glacier ice at the location where basal ice crops out on the ice surface. Hooke also suggested that debris from the ice-cored moraine may be recycled onto the superimposed ice and overridden by the glacier to produce complex structures at the ice margin. This account of the overriding of superimposed ice and recycling of debris from ice-cored moraines is the foundation of the apron entrainment model.

[20] Although the gentle dome-shaped form of the margin of the Barnes Ice Cap is quite different from the cliff of Victoria Upper Glacier there are some strong structural similarities between the ice margins. At Barnes Ice Cap the location of the inner moraine, between the ice of meteoric-origin and superimposed ice, is similar to the location of the basal ice at Victoria Upper Glacier, which occurs between the apron and the ice of meteoric origin ice in the cliff (Figure 11). However, at Victoria Upper Glacier the basal ice is associated with patches of debris (Figure 2) rather than an ice-cored moraine because of the relatively low debris concentrations and the low emergence velocity of the basal zone.

[21] Although Shaw's apron entrainment model is founded on Hooke's work, in Shaw's model the basal ice is derived from the apron [*Shaw*, 1977], whereas at the Barnes Ice Cap Hooke made a clear distinction between the basal ice and the overridden superimposed ice. Shaw suggested four lines of evidence supporting interpretation of the basal ice as the product of apron overriding:

[22] 1. The bubbly appearance and foliation of the ice, which was attributed to air trapped in the apron and the extension of crudely stratified material that accumulates on the apron.

[23] 2. The relative sorting of the debris, which he attributed to sediments that accumulate on the apron.

[24] 3. The approximate conformity of the top of the basal debris zone and the height of the apron.

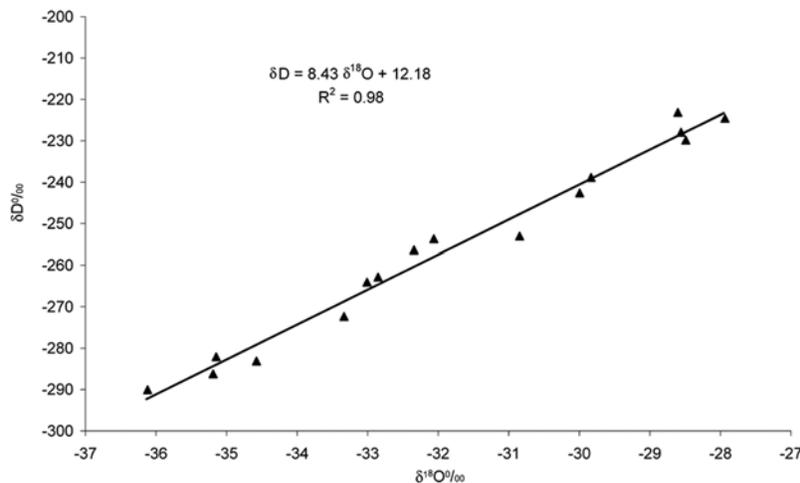[25] 4. Tilting of terraces, which he attributed to overturning of the apron.

Figure 9. A δD-$\delta^{18}O$ diagram showing samples taken from a series of short cores distributed over the ablation zone of the glacier. All samples were taken from 1 m below the glacier surface.
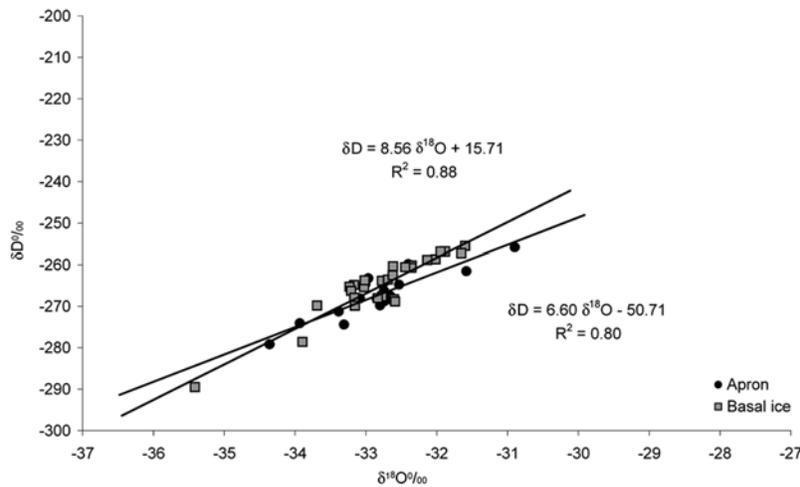
Figure 10. A δD-δ^{18}O diagram showing samples from the apron and basal ice. The regression line for the apron ice plot on the line δD = 6.60 δ^{18}O − 50.71 (r^2 = 0.80, slope standard error ± 0.16), which is statistically significantly different from regression line from the basal ice samples (δD = 8.56 δ^{18}O + 15.71, r^2 = 0.88, slope standard error ± 0.10).

[26] These arguments, however, may not be as compelling as initially thought. For example, the presence of gas bubbles is not direct evidence of apron entrainment because many types of basal ice contain gas [e.g., *Hubbard and Sharp*, 1989; *Lorrain et al.*, 1999]. Similarly the presence of foliation cannot be regarded as definitive evidence of this process because foliation in basal ice occurs wherever basal ice containing debris is deformed [*Hubbard and Sharp*, 1989; *Knight*, 1997]. The relatively well-sorted nature of the debris in basal ice provides, at best, ambiguous evidence of the derivation of basal ice from the apron because the apron is not the only source of well-sorted sediments in the dry valleys. The beds of several glaciers appear to be dominated by fluvial sediments [*Fitzsimons et al.*, 2000]. In addition our observations show that there is no conformity between the top of the basal debris zone and the top of the apron because the top of the apron is consistently below the top of the basal zone (Figure 3). We interpret the presence of the top of the apron below the top of the basal zone as evidence of the development of an accumulation slope, which is being overridden by the glacier (Figure 11), which means that the top of the basal ice is above the top of the apron. Finally, the tilting of terraces at glacier margins in the McMurdo dry valleys is a product of proglacial glaciotectonic deformation [*Fitzsimons*, 1996; *Lorrain et al.*, 1999], which may be accompanied by apron formation and deformation, but the two are not necessarily coupled.

[27] Shaw's work on the margins of cold-based glaciers in the McMurdo dry valleys was followed by a model for the structural evolution of glacier margins by *Chinn* [1991]. This model describes a sequence of ice advance leading to apron overriding, deformation of the overridden ice and debris which is recycled at the base of the glacier to be "regurgitated" as a "shear moraine" [*Chinn*, 1991, Figure 4]. Here the use of the term "shear moraine" seems similar to the term "inner moraine" used by others [e.g., *Weertman*, 1961; *Hooke*, 1973]. However, our data suggest this model is incorrect because we can demonstrate that the basal ice is compositionally distinct from the apron ice. In addition our observations in the tunnel suggest that although the apron ice is deforming, there is no visible evidence for the presence of a distinct shear zone. However, differences in the viscosity of basal ice and overridden apron ice at Meserve Glacier [*Cuffey et al.*, 2000b, Figure 2] show that basal ice deforms more rapidly than overridden apron ice, which could be viewed as evidence of the presence of an indistinct shear zone (K. M. Cuffey, personal communication, 2007).

[28] Although both *Shaw* [1977] and *Chinn* [1991] state that the boundary between the basal ice and the apron occurs at the foot of the terminal cliff, our surface and subsurface data demonstrate that the boundary crops out on the upper part of the apron. It appears that Shaw's and Chinn's observations are erroneous because they relied on

Table 4. Isotopic Data From Surface, Apron, and Basal Ice Samples Expressed As Parts per Thousand Deviation From Vienna Standard Mean Ocean Water

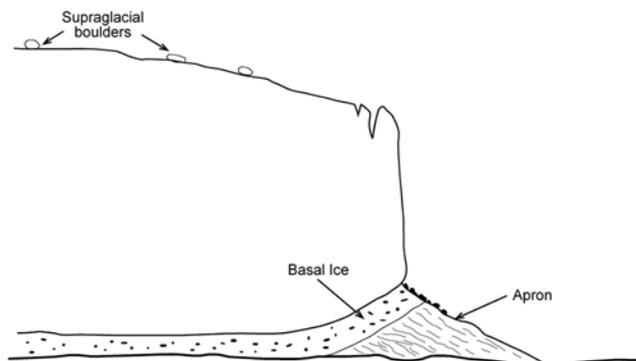|	δ^{18}O				δD				
	Minimum	Maximum	Mean	SD[a]	Minimum	Maximum	Mean	SD	n
Surface, ‰	−36.2	−27.8	−31.8	0.03	−289.6	−235.7	−254.1	0.47	16
Apron, ‰	−34.4	−30.9	−32.8	0.79	−289.4	−255.6	−267.4	5.79	17
Basal, ‰	−35.5	−31.6	−32.7	0.78	−289.5	−255.8	−265.1	7.14	27

[a]SD, standard deviation.

Figure 11. Interpretative model of the margin of Victoria Upper Glacier showing the basal ice flowing from a subglacial source and over the marginal apron. The overridden apron forms a second debris-bearing ice type.

surface observations. Closer inspection of the subsurface structure has demonstrated surface icings often conceal the contact between basal ice and the overridden apron (Figure 5).

[29] Observations of ice margins in the Canadian Arctic present a quite different view of the process of apron formation, deformation and overriding. Here it appears that aprons can be overridden and entrained together with ice marginal fluvial sediment and stagnant ice during ice advances [*Evans*, 1989, Figure 10] or when glaciomarine sediments are thrust by advancing ice, and the sediment blocks are subsequently entrained by the advancing glacier terminus [*Evans*, 1989, Figure 11]. Both of these conditions describe ice marginal glaciotectonic deformation processes that appear to operate in conjunction with cliff collapse to produce a compound apron similar to that observed at Suess Glacier in the McMurdo dry valleys [*Fitzsimons*, 1996].

[30] The three studies reported above demonstrate that aprons are compound features that reflect the variety of materials and glaciological processes at glacier margins. All these studies, together with the observations from this study, provide evidence that basal ice can form as a result of the overriding and entrainment of proglacial aprons. However, our data are not consistent with the entrainment models proposed by *Shaw* [1977] and *Chinn* [1991] because we find no evidence to support the interpretation that the basal ice that crops out at the foot of these glaciers is derived from apron overriding. Conversely, we find several lines of evidence to suggest that there are two distinct basal ice types present at the margin of Victoria Upper Glacier: one from subglacial entrainment of the glacier substrate and one from apron entrainment.

[31] Three main points of geomorphological interest emerge from this study. Firstly, the basal ice observed at glacier margins in the McMurdo dry valleys cannot be solely attributed to the overriding and entrainment of aprons. The notion that debris contained in the basal zones of cold-based glaciers forms only from apron entrainment is contradicted by the results of this study. Furthermore, the presence of debris-bearing basal ice demonstrates that these glaciers erode at least sufficient quantities of material to form their basal ice layers. Although this study has not

provided any direct evidence of how this subglacial erosion occurs, an important clue is provided by the presence of frozen blocks of sediment in the basal ice. These blocks suggest that the source of at least some of the sediment entrained at the base of the glacier, are overridden fluvial sediments. Such sediment may be entrained because ice-rich sediment can experience deformation and entrainment if overridden by ice [*Fitzsimons*, 2006]. Alternatively, it is possible the material has been entrained by the upward migration of pore water through sediments to the glacier sole, although this requires the presence of liquid water beneath the glacier bed [e.g., *Christoffersen and Tulaczyk*, 2003; *Souchez et al.*, 2004]. Interpretation of basal ice as the product of subglacial erosion beneath a cold-based glacier is inconsistent with recent studies of landscapes that were glaciated during the Quaternary period. For example *Kleman* [1994] and *Kleman et al.* [2006] argue that unconsolidated sediments survive glaciation by cold-based ice and *Coglan et al.* [2002] and *Briner et al.* [2003, 2006] describe situations in which tors have been preserved despite a complex history of exposure, burial and limited glacial erosion associated with cold-based ice. Resolution of the conflicting views of glacial erosion beneath cold-based ice may lie in recognition that the nature of the glacier substrate acts as an independent control on erosion and entrainment processes. Strong beds such as crystalline bedrock or frozen coarse sediments may be characterized by low rates of erosion, whereas sedimentary beds that contain substantial volumes of ice (e.g., overridden permafrost) may be susceptible to deformation and entrainment by cold-based glaciers. Testing this hypothesis requires observation of the ice-substrate conditions beneath cold glaciers.

[32] The second point of interest to emerge from this study is that the landforms produced at ice margins in the McMurdo dry valleys are likely to preserve sediments from both ice types. Consequently, preservation of structures from basal ice may result in stacking of subglacially derived sediments over sediment entrained at the ice margin. Such sediments may also be characterized by an angular unconformity between the two ice types.

[33] Thirdly, the presence of the apron clearly has implications for the behavior of the glacier terminus because it forms an impediment to flow that results in compression and upwarping of the basal zone of the glacier as it is forced over the apron. Such compression may be linked to the warping and shortening of deltaic sediments that is evident beneath the apron in the GPR profiles.

5. Conclusions

[34] Ice and debris aprons are common at the front of high-latitude glaciers. They consist of a mixture of ice from cliff calving, refrozen melt water, debris from the glacier, eolian sediment, and the products of proglacial deformation. Isotopic and solute data show that at Victoria Upper Glacier the apron and basal ice are compositionally distinct from each other and that the two types of ice are not genetically linked. This interpretation is supported by surface and subsurface structural data, which show that the basal ice is derived from subglacial processes, whereas the apron is a glacier margin phenomenon. This conclusion is at odds with previous interpretations of apron behavior published by

Shaw [1977], and *Chinn* [1991]. Although we conclude that the basal ice is not derived from apron overriding, this does not preclude the operation of the apron entrainment process per se. However, apron overriding is likely to produce a stratified ice of limited horizontal extent and a wedge-shaped geometry.

References

Briner, J. P., G. H. Miller, P. T. Davis, P. R. Bierman, and M. Caffee (2003), Last Glacial Maximum ice sheet dynamics in arctic Canada inferred from young erratics perched on ancient tors, *Quat. Sci. Rev.*, *22*, 437–444, doi:10.1016/S0277-3791(03)00003-9.

Briner, J. P., G. H. Miller, P. T. Davis, and R. C. Finkel (2006), Cosmogenic radionuclides from fiord landscapes support differential erosion by ice sheets, *Geol. Soc. Am. Bull.*, *118*, 406–420, doi:10.1130/B25716.1.

Chinn, T. J. H. (1991), Polar glacier margin and debris features, *Mem. Soc. Geol. It.*, *46*, 25–55.

Christoffersen, P., and S. Tulaczyk (2003), Thermodynamics of basal freeze-on: Predicting basal and subglacial signatures of stopped ice streams and interstream ridges, *Ann. Glaciol.*, *36*, 233–243.

Coglan, P. M., P. R. Bierman, D. M. Mickelson, and M. Caffee (2002), Variation in glacial erosion near the southern margin of the Laurentide Ice Sheet, south-central Wisconsin, USA: Implications for cosmogenic dating of glacial terrains, *Geol. Soc. Am. Bull.*, *114*, 1581–1591.

Cuffey, K. M., H. Conway, A. M. Gades, B. Hallet, R. Lorrain, J. P. Severinghaus, E. J. Steig, B. Vaughn, and J. W. C. White (2000a), Entrainment at cold glacier beds, *Geology*, *28*, 351–354.

Cuffey, K. M., H. Conway, A. Gades, B. Hallet, C. F. Raymond, and S. Whitlow (2000b), Deformation properties of subfreezing glacier ice: Role of crystal size, chemical impurities, and rock particles inferred from in situ measurements, *J. Geophys. Res.*, *105*, 27,895–27,916.

Donnelly, T., S. Waldron, A. Tait, J. Dougans, and S. Bearhop (2001), Hydrogen isotope analysis of natural abundance and deuterium-enriched waters by reduction over chromium on-line to a dynamic dual inlet isotope-ratio mass spectrometer, *Rapid Commun. Mass Spectrom.*, *15*, 1297–1303.

Evans, D. (1989), Apron entrainment at the margins of sub-polar glaciers, north-west Ellesmere Island Canadian high arctic, *J. Glaciol.*, *35*, 317–324.

Farquhar, G. D., B. K. Henry, and J. M. Styles (1997), A rapid on-line technique for determination of oxygen isotope composition of nitrogen-containing organic matter and water, *Rapid Commun. Mass Spectrom.*, *11*, 1554–1560.

Fitzsimons, S. (1996), Formation of thrust-block moraines at the margins of dry-based glaciers, South Victoria Land, Antarctica, *Ann. Glaciol.*, *22*, 68–74.

Fitzsimons, S. (2006), Mechanical behaviour and structure of the debris-rich basal ice layer, in *Glacier Science and Environmental Change*, edited by P. Knight, pp. 329–335, Blackwell Sci., Malden, Mass.

Fitzsimons, S., R. Lorrain, and M. Vandergoes (2000), Behaviour of subglacial sediment and basal ice in a cold glacier, *Geol. Soc. Spec. Publ.*, *176*, 181–190.

Goldthwait, R. P. (1971), Restudy of Red Rock ice cliff in Nunatarssuaaq, Greenland, *CRREL Tech. Rep. 224*, 27 pp., U.S. Army Corps of Eng., Cold Reg. Res. and Eng. Lab., Hanover, N.H.

Hambrey, M. J., and F. Muller (1978), Structures and ice deformation in the White Glacier, Axel Heiberg Island, Northwest territories, Canada, *J. Glaciol.*, *20*, 41–66.

Hambrey, M. J., A. G. Milnes, and H. Siegenthaler (1980), Dynamics and structure of Griesgletscher, Switzerland, *J. Glaciol.*, *25*, 215–228.

Holdsworth, G. (1969), Structural geology of Meserve Glacier, Antarctica, *Antarct. J.U.S.*, *4*, 126–128.

Holdsworth, G. (1974), Meserve Glacier, Wright Valley, Antarctica: part I. Basal processes, *Rep. 37*, 104 pp. Inst. of Polar Stud., Ohio State Univ., Columbus, Ohio.

Hooke, R. L. (1973), Flow near the margin of the Barnes Ice Cap, and the development of ice-cored moraines, *Geol. Soc. Am. Bull.*, *84*, 3929–3948.

Hubbard, B., and M. J. Sharp (1989), Basal ice formation and deformation: A review, *Prog. Phys. Geogr.*, *13*, 529–558.

Jouzel, J., and R. A. Souchez (1982), Melting-refreezing at the glacier sole and the isotopic composition of the ice, *J. Glaciol.*, *28*, 35–42.

Kleman, J. (1994), Preservation of landforms under ice sheets and ice caps, *Geomorphology*, *9*, 19–32.

Kleman, J., C. Hattestrand, A. P. Stroeven, K. N. Jansson, H. De Angelis, and I. Borgström (2006), Changing glaciers and their role in earth surface interactions, in *Glacier Science and Environmental Change*, edited by P. Knight, pp. 199–200, Blackwell Sci., Malden, Mass.

Knight, P. G. (1997), The basal layer of glaciers and ice sheets, *Quat. Sci. Rev.*, *16*, 975–993.

Koerner, R. M. (1989), Ice core evidence for extensive melting of the Greenland ice sheet in the Last Interglacial, *Science*, *244*, 964–968.

Lehmann, M., and U. Siegenthaler (1991), Equilibrium oxygen- and hydrogen-isotope fractionation between ice and water, *J. Glaciol.*, *37*, 23–26.

Lorrain, R., S. Fitzsimons, M. Vandergoes, and M. Stievenard (1999), Ice composition evidence for the formation of basal ice from lake water beneath a cold-based Antarctic glacier, *Ann. Glaciol.*, *28*, 277–281.

Ramsay, J. G. (1967), *Folding and Faulting of Rocks*, 568 pp., McGraw-Hill, New York.

Rozanski, K., L. Araguds-Araguds, and R. Gonfiantini (1993), Isotopic patterns in modern global precipitation, in *Climate Change in Continental Isotopic Records, Geophys. Monogr. Ser.*, vol. 78, edited by P. K. Swart et al., pp. 1–36, AGU, Washington, D.C.

Sharp, M. (1984), Annual moraine ridges at Skalafellsjokull, south-east Iceland, *J. Glaciol.*, *30*, 82–93.

Sharp, M., W. Lawson, and R. S. Anderson (1988), Tectonic processes in a surge-type glacier, *J. Struct. Geol.*, *10*, 499–515.

Sharp, M., J. Jouzel, B. Hubbard, and W. Lawson (1994), The character, structure and origin of the basal ice layer of a surge-type glacier, *J. Glaciol.*, *40*, 327–340.

Shaw, J. (1977), Till body morphology and structure related to glacier flow, *Boreas*, *6*, 189–201.

Souchez, R., and J. Jouzel (1984), On the isotopic composition in δD and δ^{18}O of water and ice during freezing, *J. Glaciol.*, *30*, 369–372.

Souchez, R. and R. Lorrain (2006), The environmental significance of deuterium excess in meteoric and non-meteoric Antarctic ice, in *Glacier Science and Environmental Change*, edited by P. Knight, pp. 179–184, Blackwell Sci., Malden, Mass.

Souchez, R., D. Samyn, R. Lorrain, F. Pattyn, and S. Fitzsimons (2004), An isotopic model for basal freeze-on associated with subglacial upward flow of pore water, *Geophys. Res. Lett.*, *31*, L02401, doi:10.1029/2003GL018861.

Sugden, D. (2006), Changing glaciers and their role in earth surface interactions, in *Glacier Science and Environmental Change*, edited by P. Knight, pp. 188–191, Blackwell Sci., Malden, Mass.

Weertman, J. (1961), Mechanism for the formation of inner moraines found near the edge of cold ice caps and ice sheets, *J. Glaciol.*, *3*, 965–978.

————————————
S. Fitzsimons, S. MacDonell, S. Mager, and N. Webb, Department of Geography, University of Otago, P.O. Box 56, Dunedin, New Zealand. (sjf@geography.otago.ac.nz)

R. Lorrain, and D. Samyn, Laboratoire de Glaciologie, Département des Sciences de la Terre et de l'Environnement, Université Libre de Bruxelles, CP 160/03, Avenue F.D. Roosevelt, 50, B-1050, Bruxelles, Belgium.